Available online at www.sciencedirect.com

ScienceDirect

Advances in Space Research 55 (2015) 1845–1854

ADVANCES IN SPACE RESEARCH (a COSPAR publication)

www.elsevier.com/locate/asr

4D-tomographic reconstruction of water vapor using the hybrid regularization technique with application to the North West of Iran

Zohre Adavi *, Masoud Mashhadi-Hossainali

Department of Geodesy and Geomatics Engineering, K. N. Toosi University of Technology, No. 1346, Vali_Asr Ave., Mirdamad Cr., Tehran, Iran

Received 22 July 2014; received in revised form 21 January 2015; accepted 23 January 2015
Available online 4 February 2015

Abstract

Water vapor is considered as one of the most important weather parameter in meteorology. Its non-uniform distribution, which is due to the atmospheric phenomena above the surface of the earth, depends both on space and time. Due to the limited spatial and temporal coverage of observations, estimating water vapor is still a challenge in meteorology and related fields such as positioning and geodetic techniques. Tomography is a method for modeling the spatio-temporal variations of this parameter. By analyzing the impact of troposphere on the Global Navigation Satellite (GNSS) signals, inversion techniques are used for modeling the water vapor in this approach. Non-uniqueness and instability of solution are the two characteristic features of this problem. Horizontal and/or vertical constraints are usually used to compute a unique solution for this problem. Here, a hybrid regularization method is used for computing a regularized solution. The adopted method is based on the Least-Square QR (LSQR) and Tikhonov regularization techniques. This method benefits from the advantages of both the iterative and direct techniques. Moreover, it is independent of initial values. Based on this property and using an appropriate resolution for the model, firstly the number of model elements which are not constrained by GPS measurement are minimized and then; water vapor density is only estimated at the voxels which are constrained by these measurements. In other words, no constraint is added to solve the problem. Reconstructed profiles of water vapor are validated using radiosonde measurements.

Keywords: GPS tomography; Hybrid; Water vapor

1. Introduction

The GPS tropospheric delay is usually divided to dry and wet parts. The dry part is precisely modeled if the atmospheric pressure is known precisely enough and this part of atmosphere is in hydrostatic equilibrium (Kleijier, 2004; Sheresta, 2003). The wet part can be computed by subtracting the modeled part from the total delay. This quantity can be converted to the Integrated Water Vapor (GPS IWV) or Precipitable Water Vapor (GPS PWV) using the existing techniques (Bevis et al., 1992). PWV is the amount of water vapor represented by the height of the column of the liquid water and IWV is the amount of water vapor at a specific direction (Bevis et al., 1992). The GPS IWV has an accuracy of 1–2 kg m^{-2} (Dodson and Baker, 1998; Rocken et al., 1997). According to the exiting results, the GPS PWV has an accuracy which is comparable to the PWV which is estimated from the radiosonde and Water Vapor Radiometer (WVR) profiles (Bevis et al., 1992; Emardson et al., 1998; Rocken et al., 1993; Tregoning et al., 1998).

The high spatio-temporal resolution and the low cost of estimating water vapor using GPS are some of the

* Corresponding author.
E-mail addresses: zohre_adavi@mail.kntu.ac.ir, zohre_adavi@yahoo.com (Z. Adavi), hossainali@kntu.ac.ir, masoud.hossainali@gmail.com (M. Mashhadi-Hossainali).

http://dx.doi.org/10.1016/j.asr.2015.01.025
0273-1177/

advantages of this technique as compared to the others such as WVR, lidar, radiosonde and solar spectrometer (Bai, 2004; Troller, 2004). This and the other advantages such as the capability of functioning in all weather conditions have turned the GPS into a valuable source of PWV observations for the Numerical Weather Prediction (NWP) models (Kuo et al., 1998; Yang et al., 1999).

Initial researches on water vapor were concentrated on the measurement of IWV and estimating the PWV from GPS measurements (Bevis et al., 1992; Boccolari et al., 2002; Jadea et al., 2005; Kurekar and Kuraishi, 2012; Rocken et al., 1995, 1997). The GPS PWV has been used for analyzing the accuracy of moisture fields which are obtained from Numerical Weather Prediction (NWP) models (Haase et al., 2003). To improve the forecasting accuracy of these models, GPS PWVs have been assimilated in NWP models too (Cucurull et al., 2004; De Pondeca and Zou, 2001; Kuo et al., 1993, 1996; Seko et al., 2011). GPS PWV time series are used for analyzing the spatio-temporal variations of water vapor on daily and seasonal time scales in climatology (Dai et al., 2002; Hagemann et al., 2003).

The GPS Slant Wet Delay (SWD) and the IWV can be used to analyze the heterogeneity of troposphere in three dimensions (Champollion et al., 2005). GPS measurements do not constraint the problem of tomographic modeling of water vapor. This is due to the limited number of satellites in common view together with number of the GPS receivers, the spatial and temporal distribution of the tomographic inputs and also the high temporal variations of water vapor (Champollion et al., 2005). Consequently, tomographic reconstruction of water vapor is an underdetermined problem. To find a solution for this problem, at first the rank deficiency of the problem should be fixed. Several methods have been proposed for this purpose. Hirahara (2000) has added horizontal and vertical constraints to the system of equations. Flores et al. (2000) formulated the tomography model using a Kalman filter and then solved the problem. Nilsson and Gradinarsky (2006) found the solution directly from the GPS phase measurement equations. Algebraic reconstruction technique is also used for reconstructing a tomographic model (Bender et al., 2011). Rohm and Bosy (2011) proposed a set of parameters which had been derived from the analysis of air flow to the corresponding system of equations. Radiosonde measurements and radio occultation profiles are two independent sets of constraints which has also been used in order to remedy the rank deficiency of the problem (Bender et al., 2011; Foelsche and Kirchengast, 2001; Xia et al., 2013). Braun and Rocken (2003) used the Raman lidar, Skone and Hoyle (2005) used single radiosonde and Champollion et al. (2005) used the standard atmosphere but, Bi et al. (2006) introduced a priori information by applying the average results of all radiosonde profiles over a certain time period for initializing tomographic model. Another research group in China uses the output of forecasts from Numerical Weather Prediction models as a priori information for tomographic processing (Song et al., 2006).

Voxel based tomography is a large scale inverse problem when the dimensions of the study area are large and a large number of GPS stations are used for reconstructing the tomographic image. Therefore, the application of iterative regularization techniques is inevitable. A-priori information or an initial filed is normally required when the iterative methods are used. Moreover, iterative methods suffer from semi-convergence problem (Chung et al., 2008). Hybrid methods are superior to iterative regularization techniques because: Hybrid methods project a large scale tomographic inverse problem to a small scale one which can be regularized then using a direct regularization technique; No a priori information or initial field is needed for solving the problem and since direct methods are used for computing regularized solution, the obtained solution is not affected by the semi-convergence problem as well.

Based on these advantages, in this research a hybrid regularization method is used for reconstructing a 4D tomographic image of water vapor density in northwest of Iran. Since NWP models are not assimilated with meteorological data in Iran, they do not provide reliable constraints for resolving the rank deficiency of the problem. On the other hand, regularization method of this research is independent of initial values. Therefore, the model parameters are solved for only at the model elements (voxels) in which the model parameters are adequately constrained by the GPS measurement. Finally, the model parameters are interpolated in voxels which are either not constrained or not adequately constrained by the GPS measurements. Reconstructed tomographic image is then validated using radiosonde measurements.

The next section of this paper discusses the tomographic modeling of a water vapor. Hybrid regularization technique is also introduced here. Section 3 introduces the study area and the tomographic model of this research. It also gives the numerical results and discusses on obtained the reconstructed 4D-tomographic image of water vapor density within the study area of this research. Reconstructed image has been verified using radiosonde profiles.

2. Methodology

2.1. Tomographic modeling

The Slant Total Delay (STD) of the GPS signals in troposphere are computed through (Bevis et al., 1994, 1992; Song et al., 2006):

$$STD = m_d(elv)\,ZHD + m_w(elv)\,ZWD \tag{1}$$

where elv is the elevation of the individual STD, ZHD and ZWD are the dry and wet components of STD in the zenith direction and $m_d(elv)$ and $m_w(elv)$ are the corresponding mapping functions. GMF mapping function is used here (Böhm et al., 2006b). The products $m_d(elv)ZHD$ and

$m_w(elv)ZWD$ are the Slant Hydrostatic and the Slant Wet Delays (SHD, SWD), respectively.

The dry part of tropospheric delay is a function of temperature and pressure at the surface of the Earth. Therefore, it can be precisely modeled using meteorological (surface) measurements (Davis et al., 1985). ZHD is computed to an accuracy better than a few millimeters if precise meteorological measurements are used in conjunction with the existing models (Bevis et al., 1992). In this paper, ZHD is computed using the following model (Saastamoinen, 1973):

$$ZHD = \frac{0.002277\,P_s}{(1 - 0.00266\cos(2\phi) - 0.00000028\,H)} \tag{2}$$

where P_s is the surface pressure in millibar, ϕ and H are the latitude and orthometric height in meters, respectively. Due to the high spatio-temporal variations of water vapor it is not possible to model the wet component of the slant total delay with high precision.

The zenith total delay (ZTD) can be computed using GPS processing software. Here, the Bernese GPS software has been used for this purpose (Dach et al., 2007). The corresponding details are reported in Adavi and Mashhadi Hossainali (2014). The SWD can be computed then using following equation:

$$SWD = m_d(elv) \cdot (ZTD - ZHD) \tag{3}$$

The relation between SWD and precipitable water vapor along the propagation path of the GPS signal (SWV) is (Ware et al., 1996):

$$SWV = \Pi(T_m) \cdot SWD \tag{4}$$

The following relation is also known between the ZWD and PWV parameters:

$$PWV = \Pi(T_m) \cdot ZWD \tag{5}$$

Also, the functional relation between PWV and IWV is as follows:

$$IWV = \rho_w PWV \tag{6}$$

Here, ρ_w is the density of liquid water, that is 1000 kg m^{-3}. The coefficient $\Pi(T_m)$ in Eqs. (4) and (5) is computed using the equation below:

$$\Pi = \left[10^{-6}(k_3/T_m + k_2')R_v\rho_w\right]^{-1} \tag{7}$$

where R_v is the specific gas constant of water vapor, that is 461.45 J Kg^{-1} K^{-1}, and the atmospheric refractivity constants k_3 and k_2' are approximately 3.7×10^5 K^2 mbar^{-1} and 17 K mbar^{-1} respectively. T_m is the weighted average of the atmospheric temperature. This parameter is computed using the following equation (Davis et al., 1985):

$$T_m = \frac{\int(e_v/T)\,dz}{\int(e_v/T^2)\,dz} \tag{8}$$

Here, e_v is the water vapor pressure and T is temperature in Kelvin. As a rough rule of thumb, coefficient Π is set approximately equal to 0.15 (Bevis et al., 1994). Nevertheless, the value of this conversion parameter varies from 0.12 to 0.18 according to the latitude, season and the weather condition in the study area (Jadea et al., 2005). Since IWV and PWV depend on the temporal and spatial variations of the atmosphere, conversion model Π is not a constant parameter as well. Moreover, the best estimate for this parameter is obtained when the climate conditions is taken into account (Emardson and Derks, 2000). In this paper the following model is used for this purpose (Sadeghi et al., 2014):

$$T_m = 75.39 + 0.7103\,T_0 \tag{9}$$

The observation equation for tomographic modeling of water vapor is given in Eq. (10) (Braun, 2004):

$$SWV = \frac{1}{\rho_w}\int_S \rho_v ds \tag{10}$$

where S is the signal path between a satellite and a receiver and ρ_v is density of water vapor in gm^{-3}. In practice observations are made in discrete form. Therefore, calculations are performed by discretizing Eq. (10). For this purpose, Eq. (10) is set up for every receiver and all of the visible satellites in every measurement epoch and troposphere is developed into a finite series of elements. The parameter ρ_v is assumed to be fixed in each element of this model. As a result, the linearized discrete form of Eq. (10) is as follows (Flores et al., 2000):

$$\mathbf{d} = \mathbf{A}\boldsymbol{\rho}_v \tag{11}$$

Vector $\mathbf{d}$ consists of the slant water vapors. $\boldsymbol{\rho}_v$ is the vector of unknown parameters and $\mathbf{A}$ is the design matrix whose dimension is $m \times n$ where m is the number of measurements and n is the number of the model elements. The parameter m depends on the selected time resolution for the model, the number of GPS stations and the number of visible satellites. The general form of this matrix is as follows (Rohm and Bosy, 2009):

$$\mathbf{A} = \begin{bmatrix} d_{11} & d_{12} & d_{13} & d_{14}\ c\ldots & cd_{1m} \\ d_{21} & d_{22} & d_{23} & d_{24} & \ldots & d_{2m} \\ \vdots & \vdots & \vdots & \vdots & \ddots & \vdots \\ d_{n1} & d_{n2} & d_{n3} & d_{n4} & \ldots & d_{nm} \end{bmatrix} \tag{12}$$

In this equation, d_{ij} is the length of ith ray which passes through jth model element and most of them are zero. The ray bending is ignored (Mendes, 1999) here. Therefore, straight lines are assumed to be used for modeling the propagation of electromagnetic waves. The design or coefficient matrix $\mathbf{A}$ depends on the geometry of the model (size of voxels) as well as the geometry of the measurements (Bender et al., 2011). The model geometry is defined according to the size and the topography of the study area subjected to some limitations such as, the vertical resolution of the model has to be selected 3 to 5 times smaller than the horizontal one (Bosy et al., 2010).

The geometry of measurements, i.e. the distribution of GPS stations and their relative positions with respect to

satellites, directly impacts the uniqueness of solution. Practically, some of the model elements are not constrained by the GPS measurements. According to Menke (2012), the system of observation equation in the problem of tomography is a mixed-determined problem and the inversion may become singular because propagated signals do not pass through some of the model elements within the area of interest. In order to avoid using a data source which is to be used for validating subsequent results, size of the model elements have been selected such that the majority of voxels are constraint by the GPS measurements. The problem is then solved only for such elements. Water vapor density is then interpolated for the remaining elements using reconstructed water vapors in the neighboring ones. In this approach, the accuracy of the reconstructed 4D-tomographic image naturally depends on the number elements which are constrained by the GPS measurements.

2.2. Regularization method

Hybrid methods are a group of regularization techniques which combine an iterative and a direct method for regularizing a large scale inverse problem. Therefore, hybrid regularization simultaneously benefits from the advantages of both direct and iterative techniques. This is done by projecting a large scale tomographic inverse problem to a small scale one which can be regularized then using a direct regularization technique. Projected solution of very small problem is then transformed back to the very large one. A hybrid technique benefits from reduced computation time and memory because of the application of the direct methods for regularizing the solution. Through the combined application of direct and iterative methods, Hybrid regularization reduces the required number of iterations and therefore, avoids the semi-convergence problem in iterative techniques (Chung et al., 2008; Hansen, 1998; Jiang et al., 2008). The method of Least-Squares QR (LSQR) is usually used in conjunction with a direct method of regularization such as Tikhonov or TSVD for this purpose (Bjork, 1988; Bjork et al., 1994; Hanke, 2001; Hansen, 1998; Jiang, 2010; Kilmer et al., 2006).

LSQR is an iterative regularization method in which the coefficient matrix $\mathbf{A}$ is firstly diagonalized using Lanczos' bidiagonalization method of the first type (LBD). The QR factorization is then used for solving the new system of simultaneous equations in which the coefficient matrix is a lower triangular bidiagonal one.

LB-Tikh is a hybrid regularization technique which benefits from the Lanczos' bidiagonalization method of the first type and solves the unknown parameters using the Tikhonov regularization technique (Jiang, 2010). The Lanczos' bidiagonalization algorithm with starting vector $\mathbf{d}$ produces a bidiagonal matrix is $\mathbf{B}_k \in R^{(k+1)\times k}$ and two matrices $\mathbf{U}_k \in R^{m\times(k+1)}$ and $\mathbf{V}_k \in R^{n\times k}$ with orthogonal columns such that:

$$\mathbf{A}\mathbf{V}_k = \mathbf{U}_{k+1}\mathbf{B}_k \tag{13}$$

where,

$$\mathbf{B}_k = \mathbf{U}_{k+1}^T \mathbf{A}\mathbf{V}_k; \quad \mathbf{B}_k = \begin{bmatrix} \alpha_1 & & & \\ \beta_1 & \alpha_2 & 0 & \\ & \beta_2 & \ddots & \\ & 0 & \ddots & \alpha_k \\ & & & \beta_k \end{bmatrix} \tag{14}$$

The columns $\mathbf{u}_1, \ldots, \mathbf{u}_{k+1}$ of $\mathbf{U}_{k+1}$ and the columns $\mathbf{v}_1, \ldots, \mathbf{v}_k$ of $\mathbf{V}_k$ are called the left and right Lanczos vectors. The Lanczos' bidiagonalization algorithm with starting vector $\mathbf{d}$ is initiated with:

$$\beta_1 = \|\mathbf{d}\|_2, \quad \mathbf{u}_1 = \mathbf{d}/\beta_1 \tag{15.1}$$

and for $k = 1, 2, \ldots$

$$\mathbf{p}^{(k)} = \mathbf{A}^T\mathbf{u}_k - \beta_k\mathbf{v}_k \tag{15.2}$$

$$\alpha_k = \|\mathbf{p}^{(k)}\|_2 \tag{15.3}$$

$$\mathbf{v}_k = \mathbf{p}^{(k)}/\alpha_k \tag{15.4}$$

$$\mathbf{q}^{(k)} = \mathbf{A}\mathbf{v}_k - \alpha_k\mathbf{u}_k \tag{15.5}$$

$$\beta_{k+1} = \|\mathbf{q}^{(k)}\|_2 \tag{15.6}$$

$$\mathbf{u}_{k+1} = \mathbf{q}^{(k)}/\beta_{k+1} \tag{15.7}$$

where $\mathbf{p}^{(k)}$ and $\mathbf{q}^{(k)}$ are two auxiliary vectors of lengths n and m, respectively.

After k steps of LBD, the original problem can be approximated by the projected LS problem (Chung et al., 2008):

$$\arg\min_{\boldsymbol{\rho}_v \in R(\mathbf{U}_k)} \|\mathbf{d} - \mathbf{A}\boldsymbol{\rho}_v\| = \arg\min_{\boldsymbol{\xi}} \|\mathbf{U}_k^T\mathbf{d} - \mathbf{B}_k\boldsymbol{\xi}\| \tag{16}$$

Here, $\boldsymbol{\rho}_v$ is the unknown vector of water vapor densities. Since the original problem is ill-posed, $\mathbf{B}_k$ may become very ill-conditioned. Therefore, a regularization method must be used for computing $\boldsymbol{\xi}$. Since the dimension of $\mathbf{B}_k$ is much smaller than $\mathbf{A}$, a direct method can be used for this purpose. In this paper, Tikhonov regularization is used for solving the projected problem (16):

$$\boldsymbol{\xi}_{Tikh}^{(k)} = \arg\min\left(\left\|(\mathbf{B}_k\boldsymbol{\xi} - \beta_1\hat{\mathbf{e}}_1^{(k+1)})\right\|_2^2 + \alpha^2\|\boldsymbol{\xi}\|_2^2\right) \tag{17}$$

where $\boldsymbol{\xi}^k$ is the regularized solution and $\mathbf{e}_1^{(k+1)} = [1 \quad 0 \quad \ldots \quad 0]^T$ has length $k+1$.

Regularized solution $\boldsymbol{\xi}^k$ is then projected to the original vector of unknown parameters ($\boldsymbol{\rho}_v^k$) using the matrix $\mathbf{V}_k$ and the transformation equation $\boldsymbol{\rho}_v^k = \mathbf{V}_k\boldsymbol{\xi}^k$. This is based on the fact that orthonormal columns of matrix $\mathbf{V}_k$ are the base vectors of the Krylov's subspace $\kappa_k(\mathbf{A}, \mathbf{d})$. As the result, in each iteration, the solution of the system of Eq. (16) is a linear combination of the vectors.

3. Numerical results and conclusions

3.1. Study area

Iran is a vast country which requires continuous monitoring of the weather due to various climates and different

climatic phenomena such as heavy precipitations in the northern parts and huge tornadoes in southern regions. Climate variability in Iran is such that the annual precipitation in some southern cities of this country does not exceed forty millimeters while precipitation more than 600 mm has been reported in the western regions. Also, due to the lack of data and an organized data acquisition system, numerical models are not assimilated with regional data acquired in Iran. For example, the number of radiosonde stations which are used to forecast the weather and climate changes, is only 14 and starting sites are non-uniformly distributed as well. Using the tomography method, these models can be improved. The permanent GPS stations as well as tomographic models can be used to establish a weather monitoring system in each region of the country, not only to improve the weather predictions, but also to increase the positioning accuracy.

In this research the northwestern part of the country has been selected due to its submontane topography, relatively dense GPS network and the existence of reasonable meteorological data in this area. Totally, 15 stations form the Iranian Permanent GPS Network (IPGN) and 10 synoptic weather stations have been selected within the study area of this research (Adavi and Mashhadi Hossainali, 2014). The only radiosonde station of this study is located in the vicinity of the Tabriz city (see Fig. 1). Dual frequency GPS measurements of 15 days from Day of Year (DOY) 300 to DOY 314 in the year 2011 are used here. According to the meteorological reports, the humidity of the study area is maximal during the time interval above.

Tomographic model of this study has a time resolution of 1hour. This follows the time resolution of the Weather Research and Forecasting Model (WRF). Consequently, the reconstructed model consists of 360 epochs. Radiosonde balloons are launched once a day at the radiosonde station of Tabriz. Therefore, the accuracy of the developed model can be checked only at fifteen successive epochs.

The height of the GPS stations varies from 1300 to 1950 meters above the Mean Seal Level (MSL) of Iran. Fig. 1 illustrates the height difference of the adopted GPS stations.

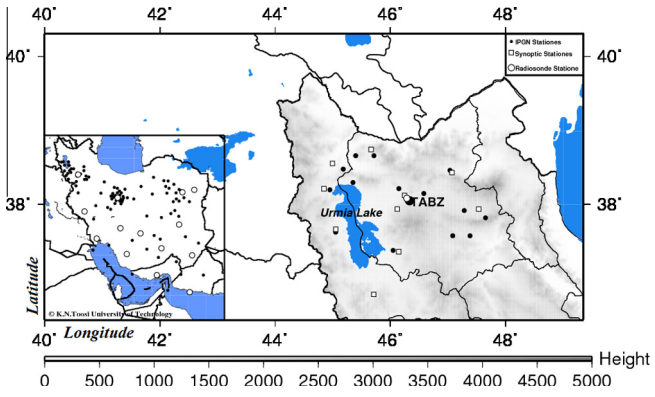

Fig. 1. Horizontal and vertical distribution of the IPGN stations in the study area of this research.

Some of the GPS stations are equipped with meteorological sensors. For the rest, the required meteorological parameters (pressure and temperature regarding Eq.2 and Eq.8) have been interpolated using technique briefly discussed below. In this study, the three-hourly synoptic data of the Iran's Meteorological Organization (IRIMO) were used together with the GPS meteo data are used for interpolation when required. Polynomial and Kriging methods are used for interpolating the pressure and temperature, respectively. Using the method of polynomial, the pressure can be interpolated with an error of ±1 h Pa. Temperature can be interpolated with an error of ±1 K, using Kiriging methods (Boer et al., 2001; Cressie, 1993; Li and Heap, 2008; Stahel et al., 2006).

3.2. Tomographic model

In this research, the resolution of the tomographic model is 40 km in horizontal direction. In the vertical direction the resolution of the model is 500 m from the surface to the height of 4 km and then, it is reduced to 1000 m. The model extends to the height of 10 km from the surface of the Earth. The concept of the model space resolution matrix is used to derive the optimum size of the voxels (Adavi and Mashhadi Hossainali, 2014).

Fig. 2a illustrates the tomographic model of this research. The spatial distribution of the GPS stations is given in Fig. 2b. According to Aster et al. (2005, p 63) the original model elements which are smeared out by the inverse solution are those whose resolution is zero or close to zero. Fig. 2a illustrates such elements in shaded form.

This resolution for the model averagely results in a tomographic image in which 91% of the model elements are constrained by the GPS measurements (see Table 1). Since the orbital period of the GPS satellite is one-half a sidereal day, i.e. 11 h and 58 min, the observation geometry is repeated 4 min earlier every day. Therefore, the number of model elements which are constrained by the GPS measurements is slightly different from day to another (see Table 1 for further details).

According to Table 1, averagely only for 9% of the model elements; the water vapor density would be the average of reconstructed parameter at neighboring blocks (elements). It should also be noted that the voxel which the radiosonde station of this study is located in as well as the voxels which are located at its top are constrained by GPS measurements.

To analyze the accuracy of a tomographic model, Root Mean Square Error (RMSE), bias and standard deviation (std) are normally used (Rohm and Bosy, 2009; Shangguan et al., 2013). These statistics are computed using the following equations (Guerova, 2003):

$$RMSE = \sqrt{\frac{1}{N}\sum_{i=1}^{N}\left(\rho_{vm}^{i} - \rho_{vo}^{i}\right)^{2}} \tag{18}$$

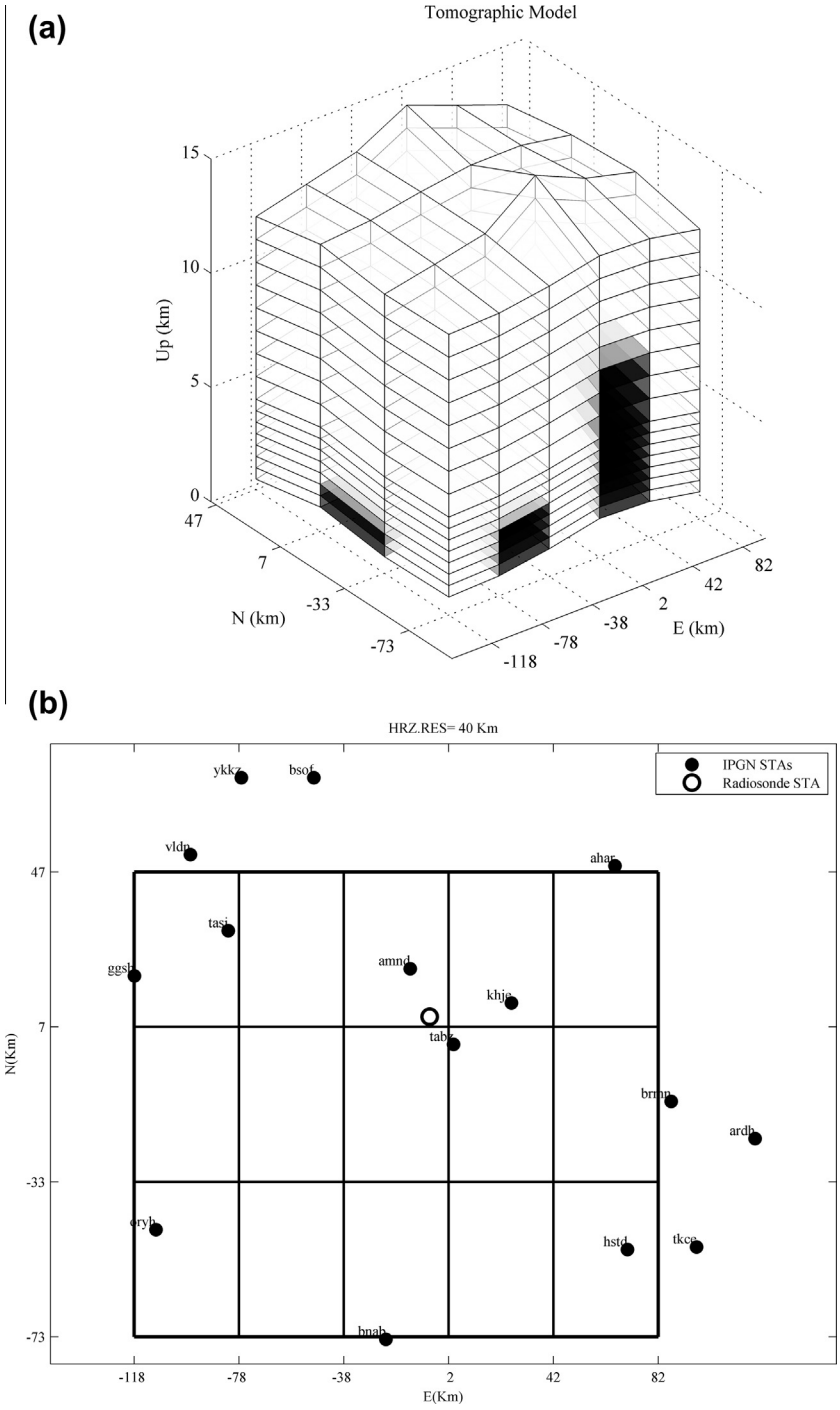

Fig. 2. The 3D-tomographic model of this research, Shaded elements illustrate some of the voxels which are not constrained by GPS measurements on DOY 300 (a). The spatial distribution of GPS stations in the first vertical layer of this model (b).

$$bias = \frac{1}{N}\sum_{i=1}^{N}\left(\rho_{vm}^{i} - \rho_{vo}^{i}\right) \tag{19}$$

$$std = \sqrt{RMSE^2 - bias^2} \tag{20}$$

Here, ρ_{vm}^{i} is the modeled water vapor density in the ith voxel and ρ_{vo}^{i} is water vapor density computed through a radiosonde profile. Moreover, N is the number of the sample elements.

3.3. Reconstructed images and accuracy analysis

A 4D-tomographic image has been reconstructed for the water vapor density in the study area of this research. To validate the obtained results, reconstructed profile of ρ_v at the position of the Tabriz radiosonde station has been compared to the corresponding profile which is obtained from the radiosonde data (Shangguan et al., 2013, 2011). Tabriz radiosonde station is the only radiosonde station

Table 1
Percent of voxels which are constrained by GPS measurements for DOY 300 to DOY 314.

DOY	Voxels with ray pass (%)	Empty voxels (%)
300	88	12
301	88	12
302	87	13
303	89	11
304	87	13
305	88	12
306	91	9
307	93	7
308	93	7
309	93	7
310	88	12
311	93	7
312	93	7
313	93	7
314	93	7
Mean	91	9

within the study area of this research. Therefore, it is not possible to check the accuracy of the reconstructed image in the other parts of this area. This analysis has been done for fifteen epochs. Fig. 3 illustrates the corresponding results and Table 2 reports on the corresponding details. Eqs. (18)–(20) have been used for this purpose. Here, the number of adapted elements is $N = 15$.

The discrepancy between radiosonde observations and the tomographic results can be due to a true error in the tomography, which can be attributed to either few slants in the developed model or instability of solution, real difference in atmospheric conditions which are sampled at different locations and times and finally true errors in the radiosonde estimates of the water vapor density (Shangguan et al., 2013). The voxel which the radiosonde station of this study is located in as well as the voxels which are located at its top are constrained by GPS measurements. This is seen through the resolution of these elements which is derived from the model space resolution matrix for the tomographic model of this research. Resolutions of these elements are almost one for all of the DOYs of this experiment. Therefore the adequacy of slants is guaranteed here. Nevertheless, distinguishing the individual contribution of the other sources in the reported bias is hard. A-priori information as to the measurement process can help understand weather the estimated bias is also contaminated by true errors in radiosonde estimates. For example,

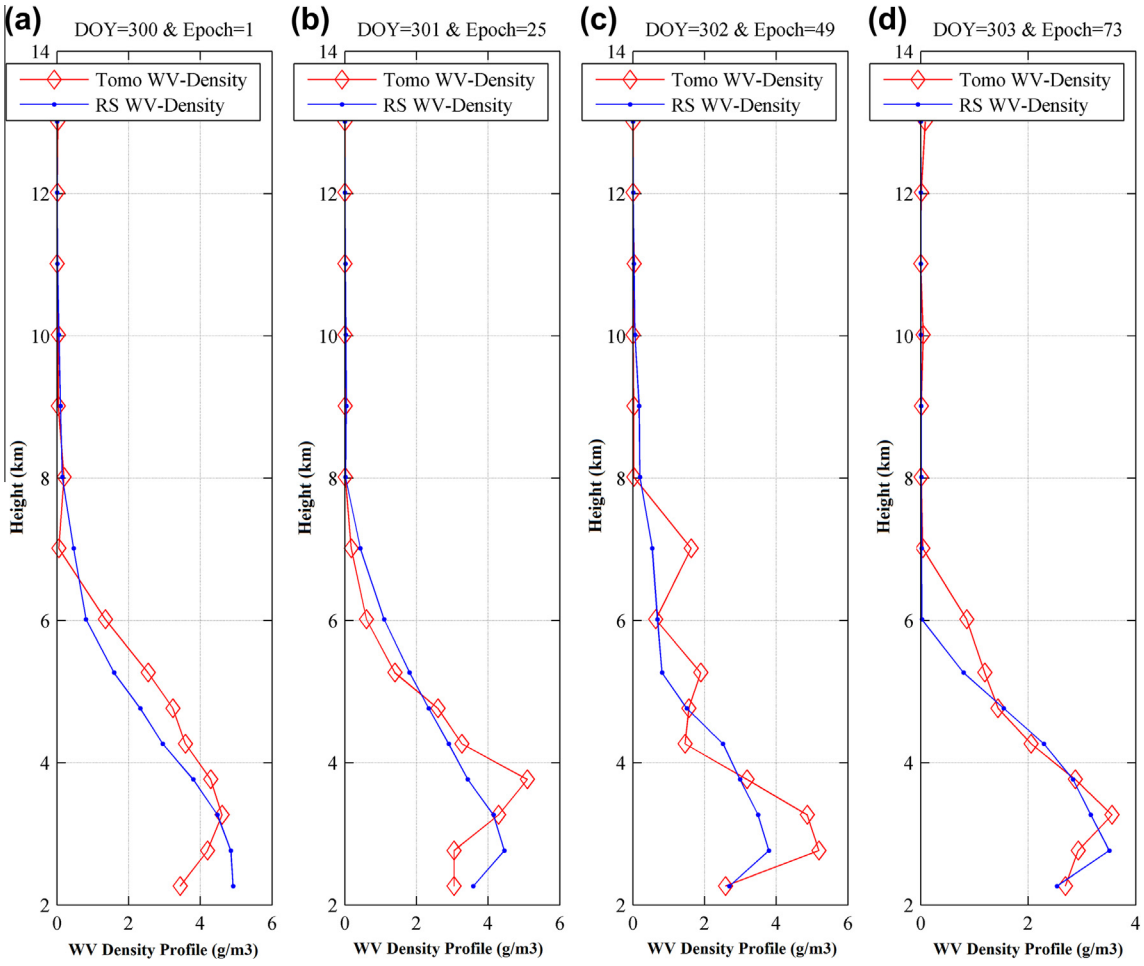

Fig. 3. The comparison of tomographic profiles to the profile derived from radiosonde data: the 1st epoch (a), the 25th epoch (b), the 49th epoch (c), the 79th epoch (d), the 265th epoch (e), the 289 h epoch (f), the 313th epoch (g) and the 317th epoch (h) (00 h : 00 min in UTC).

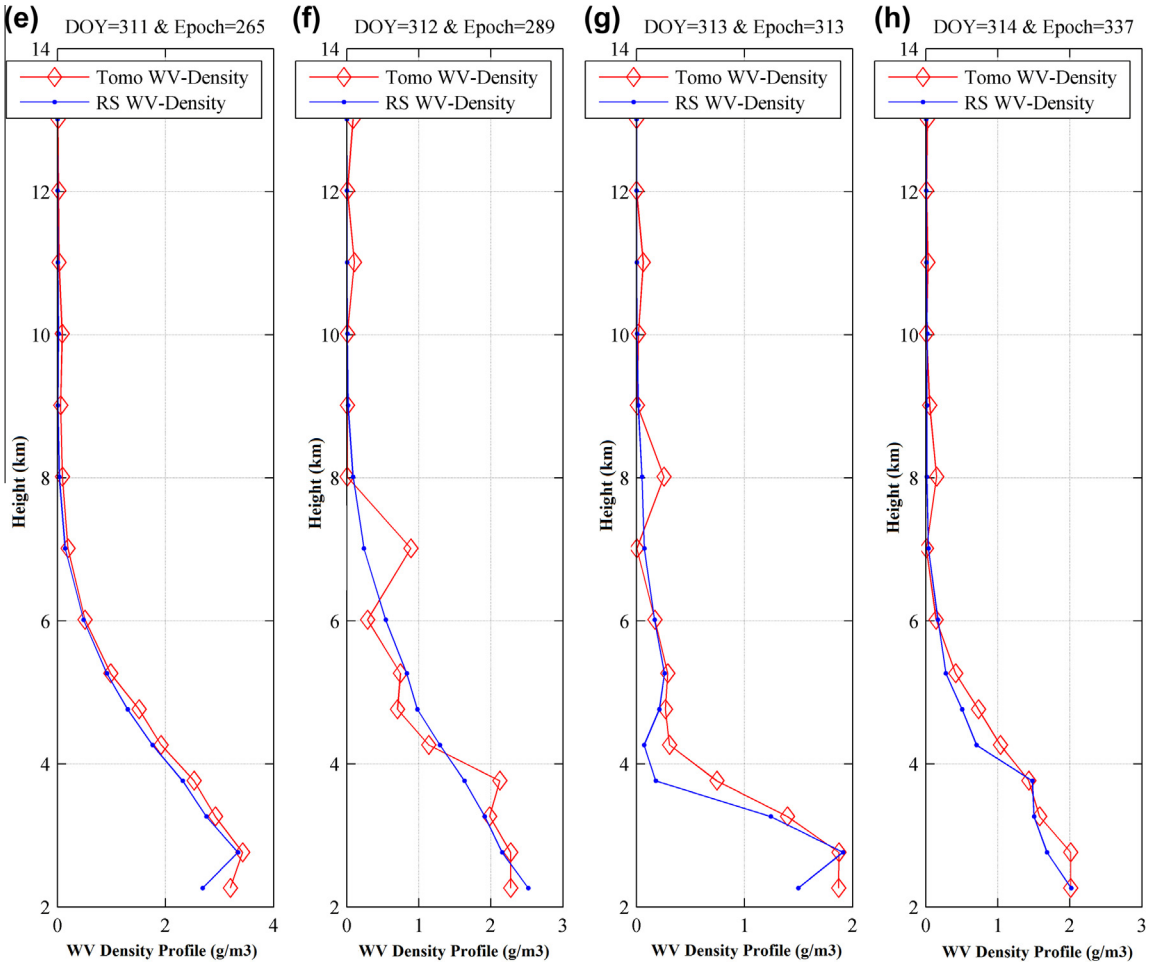

Fig 3. *(continued)*

Table 2
RMSE, bias and std for fifteen successive epoch.

DoY	RMSE (g/m^3)	Std (g/m^3)	Bias (g/m^3)
300	0.6042	0.5999	0.0724
301	0.6182	0.6161	−0.0511
302	0.7015	0.6570	0.24578
303	0.3097	0.3018	0.06977
304	0.6627	0.6557	0.09639
305	0.4692	0.4593	0.09582
306	0.4119	0.3898	0.13323
307	0.6253	0.6042	0.16122
308	0.5278	0.5269	−0.03011
309	0.6267	0.6164	0.11302
310	0.5343	0.4863	0.22141
311	0.1711	0.1259	0.11582
312	0.2506	0.2491	0.02806
313	0.2011	0.1668	0.11224
314	0.1495	0.1211	0.08763
Mean	0.4290	0.4110	0.0919

according to Iran's Meteorological Organization (IRIMO), the radiosonde temperature and humidity sensors are calibrated before launching a radiosonde balloon. This is known as the ground check. Improper calibration of the sensors results in a systematic error in the outputs. The corresponding bias decreases as the height of the sensors increases. Such a bias has been committed in the Tabriz radiosonde station at DOY 301 and DOY 302. Nevertheless, the ground check process has been perfectly done at DOY 300. Therefore, the existing discrepancy between the estimated biases (See Table 1) in DOYs 301 and 302 should be partially assigned to the true errors in radiosonde results. The stability of solution is computed in three steps. At first the *ZTD* errors are propagated to the *ZWDs*. For the data of this experiment $\sigma_{\max}(ZTD) = \pm 4$ mm according to the GPS processing results. Therefore, assuming that $\sigma_{\max}(ZHD) = \pm 1$ mm one can conclude that $\sigma_{\max}(ZWD) = \pm 4.1$ mm. Then the *ZWD* errors are propagated to *SWDs*. *ZWDs* are transformed to *SWDs* using the GMF mapping function, i.e. $SWD = GMF(z, \varphi, \lambda, h) \cdot ZWD$. In this research, the maximal value of this function is 11. Therefore, $\sigma_{\max}(SWD) = \pm 45.1$ mm. Finally, the *SWD* errors are propagated to *SWVs*. *SWD* is transformed to *SWV* using $SWV = \Pi SWD$ where Π takes the maximal value of 0.15 within the study area of this research. Therefore, $\sigma_{\max}(SWV) = \pm 6.5$ mm. Using the regularization parameter which suggests the best solution for a certain

day and at a certain epoch (here, the first daily epochs of this experiment), the $GPS-SWVs$ are iteratively changed using the formulae: $GPS\_SWV_{new} = GPS\_SWV \pm 6.5\,\alpha$ where $0 \leqslant \alpha \leqslant 1$. According to the obtained results, when this addition term reaches 7.22 mm, the stability of solution is better than 1 gr/m^3.

4. Concluding remarks

This study is the first attempt to address the tomographic reconstruction problem of water vapor in Iran. The north western part of the country has been considered as the study area in this research due to submontane topography, relatively dense GPS network and the existence of reasonable meteorological data in this area. Hybrid regularization is used for reconstruction a 4D-tomographic image of water vapor density in this area. No initial value is required in this regularization technique. Appropriate selection of the model resolution has minimized the number of elements which are not constrained by GPS measurements. As a result, the problem is solved only for the voxels which are constrained by the GPS measurements. For the voxels which are not constrained by GPS measurements, water vapor density is assumed to be the average of this quantity in the surrounding ones. The accuracy of the reconstructed image has been analyzed using the only radiosonde station within the study area of this research. According to the obtained results, the RMSE or precision of reconstructed images for the 15 days period of this experiment is expected on average to be 0.53 gr/m^3. The bias of this model is expected on average to be 0.1 gr/m^3. Based on the computed variations for the *SWVs* the stability of the model is derived. The stability of the tomographic model of this research is expected to be 1 gr/m^3.

Acknowledgments

During this research, Mr. Akbar who is a member of the meteorological organization of Iran, kindly provided us valuable remarks. His cooperation is appreciated here. The meteorological organization of Iran provided the radiosonde profiles with dense pressure levels of the Tabriz station and the observation files of synoptic stations in the north-western part of the country for this research. This collaboration is also appreciated here. We are grateful to the National Cartographic Center (NCC) of Iran for providing the observation files of the Azarbayjan sub-network of the Iranian Permanent GPS Network too.

References

Adavi, Z., Mashhadi Hossainali, M., 2014. 4D-tomographic reconstruction of the tropospheric wet refractivity using the concept of virtual reference station, case study: North West of Iran. Meteorol. Atmos. Phys., 125

Aster, R., Borchers, B., Thurber, C., 2005. Parameter estimation and inverse problems, vol. 90. Elsevier Academic Press, USA.

Bai, Z., 2004. Near-real-time GPS sensing of atmospheric water vapour (Ph.D.). Queensland University of Technology.

Bender, M., Dick, G., Ge, M., Deng, Z., Wickert, J., Kahle, H.-G., Raabe, A., Tetzlaff, G., 2011. Development of a GNSS water vapour tomography system using algebraic reconstruction techniques. Adv. Space Res. 47, 1704–1720.

Bevis, M., Businger, S., Chiswell, S., 1994. GPS meteorology: mapping zenith wet delays on to precipitable water. J. Appl. Meteorol. 33, 379–386.

Bevis, M., Businger, S., Herring, T., Rocken, C., Anthes, R.A., Ware, R.H., 1992. GPS meteorology: remote sensing of atmospheric water vapor using the global positioning system. J. Geophys. Res. 97 (D14), 15787–15801.

Bi, Y., Mao, J., Li, C., 2006. Preliminary results of 4-D water vapor tomography in the troposphere using GPS. Adv. Atmos. Sci. 23, 551–560.

Bjork, A., 1988. A bidiagonalization algorithm for solving large and sparse ill-posed systems of linear equations. BIT 28, 659–670.

Bjork, A., Grimme, E., van Dooren, P., 1994. An implicit shift bidiagonalization algorithm for ill-posed systems of linear equations. BIT 34, 510–534.

Boccolari, M., Fazlagic, S., Frontero, P., Lombroso, L., Pugnaghi, S., Santangelo, R., Corradini, S., Teggi, S., 2002. GPS zenith total delays and precipitable water in comparison with special meteorological observations in Verona (Italy) during MAP-SOP. Ann. Geophys. 45.

Boer, E.P.J., Beurs, K.M.D., Hartkamp, A.D., 2001. Kriging and thin plate splines for mapping climate variables. JAG 3.

Böhm, J., Niell, A., Tregoning, P., Schuh, H., 2006b. Global mapping function (GMF): a new empirical mapping function based on numerical weather model data. Geophys. Res. Lett. 33.

Bosy, J., Rohm, W., Sierny, J., 2010. The concept of the near real time atmosphere model based on the GNSS and the meteorological data from the ASG-EUPOS reference stations. Acta Geodyn. Geomater. 7, 253–261.

Braun, J., Rocken, C., 2003. Water vapor tomography within the planetary boundary layer using GPS. International Workshop on GPS Meteorology, Tsukuba, Japan, 3-09-1-4.

Braun, J.J., 2004. Remote sensing of atmospheric water vapor with the global positioning system (Ph.D.). University of Colorado.

Champollion, C., Masson, F., Bouin, M.N., Walpersdorf, A., Doerflinger, E., Bock, O., van Baelen, J., 2005. GPS water vapour tomography: preliminary results from the ESCOMPTE field experiment. Atmos. Res. 74, 253–274.

Chung, J., Nagy, J.G., O'Leary, D.P., 2008. A weighted GCV method for Lanczos hybrid regularization. Electron. Trans. Numer. Anal. 28, 149–168.

Cressie, N., 1993. Statistics for Spatial Data. Wiley, New York.

Cucurull, L., Vandenberge, F., Barker, D., Vilaclara, E., Rius, A., 2004. Threedimensional variational data assimilation of ground-based GPS ZTD and meteorological observations during the 14 December 2001 storm event over the western mediterranean sea. Mon. Weather Rev. 132, 749–763.

Dach, R., Hugentobler, U., Fridez, P., Meindl, M., 2007. Bernese GPS Software Version 5.0. Astronomical Institute, University of Bern.

Dai, A., Wang, J., Ware, R.H., Van Hove, T., 2002. Diurnal variation in water vapor over North America and its implications for sampling errors in radiosonde humidity. J. Geophys. Res. 107.

Davis, J.L., Herring, T.A., Shapiro, I.I., Rogers, E.E., Elgered, G., 1985. Geodesy by radio interferometry: effects of atmospheric modeling errors on estimates of baseline length. Radio Sci. 20 (6), 1593–1607.

de Pondeca, M., Zou, Z., 2001. A case study of the variational assimilation of GPS zenith delay observations into a mesoscale model. J. Appl. Meteorol. 40, 1559–1576.

Dodson, A.H., Baker, H.C., 1998. Accuracy of orbits of GPS atmospheric water vapour estimation. Phys. Chem. Earth 23, 119–124.

Emardson, T.R., Derks, H.J.P., 2000. On the relation between the wet delay and the integrated precipitable water vapour in the European atmosphere. Meteorol. Appl. 7, 61–68.

Emardson, T.R., Elgered, G., Johansson, J.M., 1998. Three months of continuous monitoring of atmospheric water vapor with a network of global positioning system receivers. J. Geophys. Res. 103, 1807–1820.
Flores, A., Ruffini, G., Rius, A., 2000. 4D tropospheric tomography using GPS slant wet delays. Ann. Geophys. 18 (2), 223–234.
Foelsche, U., Kirchengast, G., 2001. Tropospheric water vapor imaging by combination of ground-based and space born GNSS sounding data. J. Geophys. Res. 106 (D21), 27221–27231.
Guerova, G., 2003. Application of GPS derived water vapour for numerical weather prediction in Switzerland (Ph.D.). University of Bern.
Haase, J., Ge, M., Vedel, H., Calais, E., 2003. Accuracy and variability of GPS tropospheric delay measurements of water vapor in the western mediterranean. J. Appl. Meteorol. 42, 1547–1568.
Hagemann, S., Bengtsson, L., Gendt, G., 2003. On the determination of atmospheric water vapor from GPS measurements. J. Geophys. Res. 108.
Hanke, M., 2001. On Lanczos based methods for the regularization of discrete ill-posed problems. BIT 41, 1008–1018.
Hansen, P.C., 1998. Rank-deficient and discrete ILL-posed problems: numerical aspect of linear inversion. Philadelphia.
Hirahara, K., 2000. Local GPS tropospheric tomography. Earth Planets Space 52 (11), 935–939.
Jadea, S., Vijayana, M.S.M., Gaura, V.K., Prabhub, P.T., Sahuc, S.C., 2005. Estimates of precipitable water vapour from GPS data over the Indian subcontinent. J. Atmos. Sol.-Terr. Phys. 65, 623–635.
Jiang, M., Xia, L., Shou, G., Liu, F., Crozier, S., 2008. Two hybrid regularization frameworks for solving the electrocardiography inverse problem. Phys. Med. Biol. 53, 5151–5164.
Jiang, Y., 2010. Solving the inverse problem of electrocardiography in a realistic environment. Karlsruher Institut of Technologie (KIT) Scientific.
Kilmer, M.E., Hansen, P.C., Espanol, M.I., 2006. A projection-based approach to general-form Tikhonov regularization. SISC.
Kleijier, F., 2004. Troposphere modeling and filtering for precise GPS leveling (Ph.D.). Delft.
Kuo, Y.-H., Guo, Y.-R., Westwater, E., 1993. Assimilation of precipitable water measurements into a mesoscale numerical model. Mon. Weather Rev. 121, 619–643.
Kuo, Y.-H., Zuo, X., Guo, Y.-R., 1996. Variational assimilation of precipitable water using nonhydrostatic mesoscale adjoint model. Mon. Weather Rev. 124, 122–147.
Kuo, Y.H., Zou, X., Huang, W., 1998. The impact of global positioning system data on the prediction of an extratropical cyclone: an observing system experiment. Dyn. Atmos. Oceans 27, 439–470.
Kurekar, R.G., Kuraishi, M.A., 2012. Determination of precipitable water vapour using global positioning system. Int. J. Geol. Earth Environ. Sci. 2, 51–57.
Li, J., Heap, A.D., 2008. A review of spatial interpolation methods for environmental scientists. Resour. Energy Tourism.
Mendes, V., 1999. Modeling the neutral-atmosphere propagation delay in radiometric space techniques (Ph.D.). University of New Brunswick, Fredericton, New Brunswick, Canada.
Menke, W., 2012. Geophysical Data Analysis: Discrete Inverse Theory MATLAB Edition, third ed. Academic Press is an imprint of Elsevier.
Nilsson, T., Gradinarsky, L., 2006. Water vapor tomography using GPS phase observations: simulation results. IEEE Trans. Geosci. Remote Sens. 44 (10 Part 2), 2927–2941.
Rocken, C., Hove, T.V., Johnson, J.M., Solheim, F., Ware, R.H., 1995. GPS/STORM-GPS sensing of atmospheric water vapor for meteorology. J. Atmos. Oceanic Technol. 12, 468–478.
Rocken, C., van Hove, T., Ware, R.H., 1997. Near real-time GPS sensing of atmospheric water vapor. Geophys. Res. Lett. 24, 3221–3224.
Rocken, C., Ware, R., van Hove, T., Solheim, F., Alber, C., Johansson, J., Bevis, M., 1993. Sensing atmospheric water vapor with the global positioning system. Geophys. Res. Lett. 20, 2631–2634.
Rohm, W., Bosy, J., 2009. Local tomography troposphere model over mountains area. Atmos. Res. 93 (4), 777–783.
Rohm, W., Bosy, J., 2011. The verification of GNSS tropospheric tomography model in a mountainous area. Adv. Space Res. 47, 1721–1730.
Saastamoinen, J., 1973. Contributions to the theory of atmospheric refraction. Part II: refraction corrections in satellite geodesy. Bull. Geod. 107, 13–34.
Sadeghi, E., Mashhadi-Hossainali, M., Etemadfard, H., 2014. Determining precipitable water in the atmosphere of Iran based on GPS zenith tropospheric delays. Ann. Geophys. 57.
Seko, H., Miyoshi, T., Shoji, Y., Saito, K., 2011. Data assimilation experiments of precipitable water vapour using the LETKF system: intense rainfall event over Japan 28 July 2008. Tellus 63A, 402–414.
Shangguan, M., Bender, M., Ramatschi, M., Dick, G., Wickert, J., Raabe, A., Gales, R., 2013. GPS tomography: validation of reconstructed 3-D humidity fields with radiosonde profiles. Ann. Geophys. 31, 1491–1505.
Shangguan, M., Bender, M., Wickert, J., Raabe, A., 2011. Validation of GNSS Water Vapour Tomography with Radiosonde Data. Geodätische Woche 2011 Nürnberg.
Sheresta, S.M., 2003. Investigations into the estimation of tropospheric delay and wet refractivity using GPS measurements (Master of Science). Calgary, Alberta, Canada.
Skone, S., Hoyle, V.A., 2005. Troposphere modeling in a regional GPS network. J. Global Position. Syst. 4, 230–239.
Song, S., Zhu, W., Ding, J., Peng, J., 2006. 3D water–vapor tomography with Shanghai GPS network to improve forecasted moisture field. Chin. Sci. Bull. 51, 607–614.
Stahel, K., Moore, R.D., Floyer, J.A., Asplin, M.G., Mckendry, I.G., 2006. Comparison of approaches for spatial interpolation of daily air temperature in a large region with complex topography and highly variable station density. Agric. For. Meteorol. 13.
Tregoning, P., Boers, R., O'Brien, D., 1998. Accuracy of absolute precipitable water vapor estimates from GPS observations. J. Geophys. Res. D: Atmos. 103 (D22), 701–710.
Troller, M., 2004. GPS based determination of the integrated and spatially distributed water vapor in the troposphere (Ph.D.). ETH Zurich.
Ware, R., Exner, M., Feng, D., Gorbunov, M., Hardy, K., Herman, B., Kuo, W., Meehan, T., Melbourne, W., Rocken, C., Schreiner, W., Sokolovskiy, S., Solheim, F., Zou, X., Anthes, R., Businger, S., 1996. GPS sounding of the atmosphere from low Earth orbit: preliminary results. Bull.-Am. Meteorol. Soc. 77, 19–40.
Xia, P., Cai, C., Liu, Z., 2013. GNSS troposphere tomography based on two-step reconstructions using GPS observations and COSMIC profiles. Ann. Geophys. 31, 1805–1815.
Yang, X., Sass, B., Elgered, G., Johansson, J.M., Emardson, T.R., 1999. A comparison of precipitable water vapor estimates by an NWP simulation and GPS observations. J. Appl. Meteorol. 38, 941–956.